

PET-CT Imaging of Polymeric Nanoparticle Tumor Accumulation in Patients

Iris H. C. Miedema, Gerben J. C. Zwezerijnen, Marc C. Huisman, Ellen Doeleman, Ron H. J. Mathijssen, Twan Lammers, Qizhi Hu, Guus A. M. S. van Dongen, Cristianne J. F. Rijcken, Danielle J. Vugts, and C. Willemien Menke-van der Houven van Oordt*


Several FDA/EMA-approved nanomedicines have demonstrated improved pharmacokinetics and toxicity profiles compared to their conventional chemotherapeutic counterparts. The next step to increase therapeutic efficacy depends on tumor accumulation, which can be highly heterogeneous. A clinical tool for patient stratification is urgently awaited. Therefore, a docetaxel-entrapping polymeric nanoparticle (^{89}Zr -CPC634) is radiolabeled, and positron emission tomography/computed tomography (PET/CT) imaging is performed in seven patients with solid tumors with two different doses of CPC634: an on-treatment (containing 60 mg m⁻² docetaxel) and a diagnostic (1–2 mg docetaxel) dose (NCT03712423). Pharmacokinetic half-life for ^{89}Zr -CPC634 is mean 97.0 ± 14.4 h on-treatment, and 62.4 ± 12.9 h for the diagnostic dose ($p = 0.003$). At these doses accumulation is observed in 46% and 41% of tumor lesions with a median accumulation in positive lesions 96 h post-injection of 4.94 and 4.45%IA kg⁻¹ ($p = 0.91$), respectively. In conclusion, PET/CT imaging with a diagnostic dose of ^{89}Zr -CPC634 accurately reflects on-treatment tumor accumulation and thus opens the possibility for patient stratification in cancer nanomedicine with polymeric nanoparticles.

1. Introduction

Docetaxel is an antimitotic drug that is active against a wide range of human cancers.^[1] Despite its clinical value, docetaxel fails to exert an antitumor effect in a substantial number of patients, with response rates ranging from 6% to 45%.^[2] This is, at least in part, caused by the high inter-patient variability in pharmacokinetics (PK), leading to insufficient exposure of docetaxel in tumor tissues.^[3] Using positron emission tomography/computed tomography (PET/CT) imaging, it was previously shown that high intratumoral concentrations of [¹¹C]-docetaxel correlated with response, suggesting that sufficient drug delivery is essential for success of therapy.^[4] Simply increasing the administered dose of docetaxel is not feasible due to the potentially life-threatening adverse events (AEs) such as severe febrile neutropenia, fluid retention, pneumonitis, and

I. H. C. Miedema, E. Doeleman, C. W. Menke-van der Houven van Oordt
Amsterdam UMC location Vrije Universiteit Amsterdam
Department of Medical Oncology
De Boelelaan 1117, Amsterdam 1081 HV, The Netherlands
E-mail: c.menke@amsterdamumc.nl

I. H. C. Miedema, G. J. C. Zwezerijnen, M. C. Huisman, E. Doeleman,
G. A. M. S. Dongen, D. J. Vugts, C. W. Menke-van der Houven van Oordt
Cancer Center Amsterdam
Imaging and Biomarkers
De Boelelaan 1117, Amsterdam 1081 HV, The Netherlands

 The ORCID identification number(s) for the author(s) of this article can be found under <https://doi.org/10.1002/adma.202201043>.

© 2022 The Authors. Advanced Materials published by Wiley-VCH GmbH. This is an open access article under the terms of the Creative Commons Attribution-NonCommercial-NoDerivs License, which permits use and distribution in any medium, provided the original work is properly cited, the use is non-commercial and no modifications or adaptations are made.

DOI: 10.1002/adma.202201043

G. J. C. Zwezerijnen, M. C. Huisman, G. A. M. S. Dongen, D. J. Vugts
Amsterdam UMC location Vrije Universiteit Amsterdam
Department of Radiology and Nuclear Medicine
De Boelelaan 1117, Amsterdam 1081 HV, The Netherlands

R. H. J. Mathijssen
Erasmus University Medical Center
Erasmus University
Erasmus MC Cancer Institute
Department of Medical Oncology
Doctor Molewaterplein 40, Rotterdam 3015 GD, The Netherlands

T. Lammers
Institute for Experimental Molecular Imaging
Helmholtz Institute for Biomedical Engineering
RWTH – Aachen University
Templergraben 55, 52062 Aachen, Germany

Q. Hu, C. J. F. Rijcken
Cristal Therapeutics
Oxfordlaan 55, Maastricht 6229 EV, The Netherlands

neuropathy.^[5] Therefore, strategies that improve the PK and intratumoral concentrations of docetaxel—without increasing the risk of severe AEs—hold great promise. To this end, various alternative approaches, including nanocarriers, are under development.^[6]

One of these nanocarriers is CPC634: a 65 nm polymeric nanoparticle based on PEG-b-pHPMAM-lactate block copolymers containing docetaxel.^[7,8] To improve its stability in the systemic circulation, this nanoparticle consists of a hydrophobic core accommodating the poorly soluble docetaxel, which via a biodegradable ester linker is temporarily crosslinked with the polymeric network. The hydrophilic dense PEG shell prevents protein adsorption, another prerequisite for prolonged circulation.^[9] Nanoparticles such as CPC634 can accumulate in tumors by making use of the enhanced permeability and retention (EPR) effect.^[10] This phenomenon occurs in solid tumors where the endothelial lining of the tumor vasculature contains fenestrations. Particles of around 10–100 nm are able to extravasate, and because of the lack of lymphatic drainage and/or due to phagocytosis by tissue-resident macrophages, they become trapped within tumors. Upon local hydrolysis of the ester linker, docetaxel will gradually diffuse out of the nanoparticle, resulting in a continuous exposure of the tumor cells. As most healthy tissues do not contain fenestrated endothelium, they remain largely unaffected. Consequently, the design of nanomedicines is aimed to increase systemic circulation, to reduce exposure of healthy tissue and thus AEs, while pursuing increased accumulation in the diseased area and thereby improving efficacy.

The recently completed phase-I trial of CPC634 already demonstrated an improved PK profile (sevenfold lower C_{max} , and an almost 300-fold lower clearance compared to conventional docetaxel) and a low frequency of life-threatening AEs when administered intravenously (i.v.) as 1-h infusion at 60 mg m⁻² with dexamethasone premedication.^[11] Another clinical study determined tumor docetaxel concentration after CPC634 and conventional docetaxel administration (both dosed 75 mg m⁻² i.v. once per 3 weeks in the same patient) in a randomized cross-over design by virtue of invasive tumor sampling. On average, a more than fourfold higher intratumoral concentration of total docetaxel was found in the tumor biopsies of patients receiving CPC634, as compared to conventionally administered docetaxel.^[12] A phase-II efficacy study in patients with platinum-resistant ovarian cancer (the CINOVA trial) of CPC634 monotherapy at 60 mg m⁻² is currently ongoing (Clinicaltrials.gov number NCT03742713).

Advances in the field of nanomedicine have resulted in several FDA-approved nanoparticles with superior PK and toxicity profiles compared to their conventional drug counterparts.^[13] The focus of the field is currently shifting toward addressing the highly heterogeneous tumor accumulation and finding ways to select those patients who will benefit most from nanomedicine treatment.^[14,15] A clinical tool that allows for patient stratification *before* starting treatment, while also providing a method to study and optimize tumor accumulation, is urgently awaited. Ideally suited for this task is PET/CT imaging: a non-invasive technique that can achieve whole-body imaging and has already shown to provide accurate quantification of radiolabeled antibodies.^[16] Here, we apply a similar approach to

⁸⁹Zr-labeled nanoparticles. A balanced nanoparticle dose—low enough to have no adverse effects and high enough to be above the threshold for rapid elimination by Kupffer cells in the liver—has the potential to enable patient stratification in clinical practice. Such a dose threshold was recently estimated to be 1.5×10^{15} nanoparticles (absolute number), based on a preclinical study performed with gold, liposomal, and silica nanoparticles.^[17]

In this clinical study, we radiolabeled CPC634 with zirconium-89 (⁸⁹Zr-CPC634), enabling its visualization and quantification with PET/CT. We compared a high on-treatment dose with a low diagnostic dose, with the primary goal to examine if the diagnostic dose correctly represents the on-treatment situation without potentially leading to adverse effects. Our secondary goal was to investigate differences in PK and biodistribution between these two doses. Ultimately the aim is to further develop diagnostic dose imaging to support patient stratification in cancer nanomedicine with polymeric nanoparticles.

2. Results and Discussion

2.1. Results

2.1.1. Radiolabeling of CPC634 Does Not Alter Its Physicochemical Properties

To enable PET imaging, [⁸⁹Zr]Zr-DFO-CPC634 (simplified as ⁸⁹Zr-CPC634) was manufactured in three steps (Figure 1a). Compared to nonlabeled CPC634, ⁸⁹Zr-CPC634 demonstrated identical results upon assessment of a defined set of physicochemical properties (including particle size, docetaxel loading content, and release kinetics; Table S1 and Figure S1, Supporting Information).

2.1.2. Radiolabeling of CPC634 Does Not Alter Preclinical PK, Biodistribution, and Tumor Accumulation

The PK evaluation consisted of two components that were measured: 1) the total docetaxel concentration, defined as the sum of released and nanoparticle-entrapped docetaxel, and reported as the percentage of the injected dose (%ID); and 2) the radioactivity concentration, reported as a percentage of the injected radioactivity of ⁸⁹Zr (%IA) and serving as a proxy for the nanocarrier component of ⁸⁹Zr-CPC634. In tumor-free mice, the %ID of total docetaxel in blood was identical for labeled and unlabeled CPC634 (Figure 1b). As expected, the radioactivity concentration in blood decreased more slowly than the total docetaxel concentration, indicating that a proportion of the docetaxel was already released from the nanoparticle and cleared from the blood, while the (now lesser filled) nanoparticle kept on circulating. In tumor-bearing mice, ex vivo analysis revealed an expected biodistribution pattern, with predominant accumulation of ⁸⁹Zr-CPC634 in liver, spleen and kidneys (Figure 1c). Moreover, the total docetaxel concentration in tumors was found to be similar for CPC634 and ⁸⁹Zr-CPC634 (Figure 1d). In conclusion, preclinical evaluation demonstrated that radiolabeling of CPC634 with ⁸⁹Zr, to enable PET imaging,

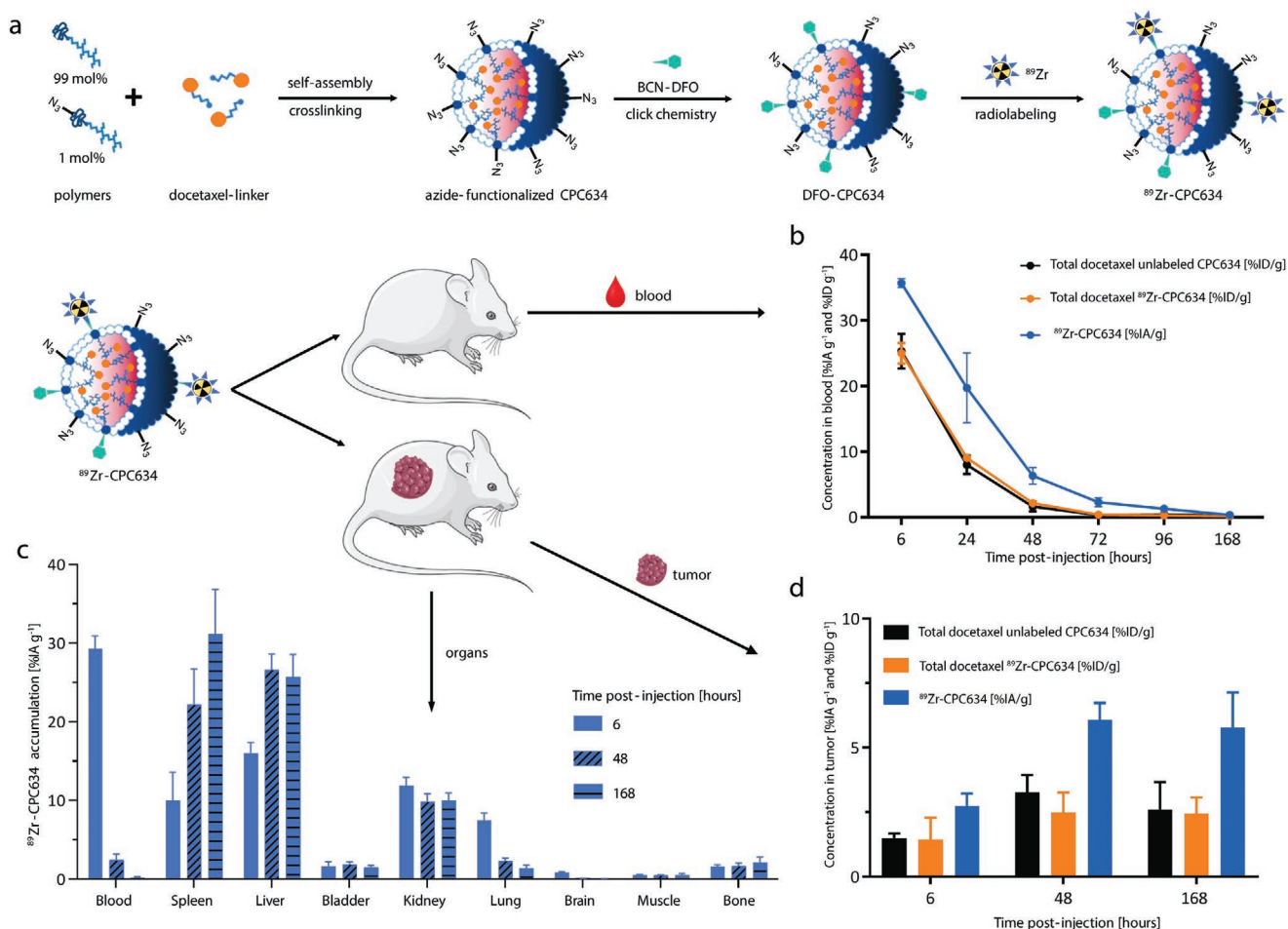


Figure 1. Radiolabeling of CPC634 and preclinical evaluation of ^{89}Zr -CPC634 in tumor-free and tumor-bearing nu/nu mice. a) Manufacturing scheme of ^{89}Zr -CPC634. b) Blood levels of total docetaxel ($\% \text{ID g}^{-1}$) and radioactivity ($\% \text{IA g}^{-1}$) at 6, 24, 48, 72, 96, and 168 h after a single injection of unlabeled CPC634 (30 mg kg^{-1}) or labeled ^{89}Zr -CPC634 (30 mg kg^{-1}) in tumor-free mice. Data are expressed as the mean \pm SD ($N = 4$). c) Ex vivo biodistribution of ^{89}Zr -CPC634 ($\% \text{IA g}^{-1}$) and d) intratumoral levels of total docetaxel ($\% \text{ID g}^{-1}$) and radioactivity ($\% \text{IA g}^{-1}$) at 6, 48, and 168 h after a single injection of unlabeled CPC634 (30 mg kg^{-1}) or ^{89}Zr -CPC634 (30 mg kg^{-1}) in mice bearing MDA-MB-231 xenografts, data are expressed as the mean \pm SD ($N = 8$). $\% \text{ID}$ = total docetaxel as a percentage of the total injected dose of CPC634-entrapped docetaxel. $\% \text{IA}$ = injected activity (only for labeled experiments), represent radioactivity as percentage of total injected radioactivity.

was done in an efficient and inert way, not affecting the PK, bio-distribution, and tumor accumulation of CPC634. The animal experiments were performed according to the NIH Principles of Laboratory Animal Care, the European Community Council Directive (2010/63/EU) for laboratory animal care and the Dutch Law on animal experimentation (“Wet op de dierproeven”, Stb 1985, 336).

2.1.3. CPC634 Treatment Is Well Tolerated

In the subsequent clinical trial, performed between July 2018 and May 2020, seven patients were included for two different setups: all patients received ^{89}Zr -CPC634 “on-treatment” (receiving 60 mg m^{-2} docetaxel, $\approx 1.8\text{--}2.2 \times 10^{16}$ nanoparticles) and five of these patients also received a low “diagnostic dose” (containing 1–2 mg docetaxel, $\approx 1.8\text{--}3.7 \times 10^{14}$ nanoparticles). Patient characteristics are summarized in Table S2 (Supporting Information). After completing the imaging procedures,

patients continued with three-weekly cycles of CPC634, until unacceptable toxicity or disease progression occurred. The CPC634 treatment was well tolerated, and the incidence and grade of observed toxicities were comparable to those previously observed during the phase-I trial.^[11] AEs are detailed in Table S3 (Supporting Information).

2.1.4. Clinical PK and Biodistribution of ^{89}Zr -CPC634 On-Treatment

To ensure to be above the dose threshold for rapid elimination and thus enable visualization of nanoparticles in tumors, patients were imaged in the on-treatment imaging protocol (Figure 2a). In short, after completing baseline 2-deoxy-2-[fluorine-18]fluoro-D-glucose (^{18}F -FDG) PET/CT, patients received the first cycle of CPC634 immediately followed by the administration of ^{89}Zr -CPC634. Subsequently, PET/CT scans were performed $\approx 24, 96,$ and 144 h post-injection.

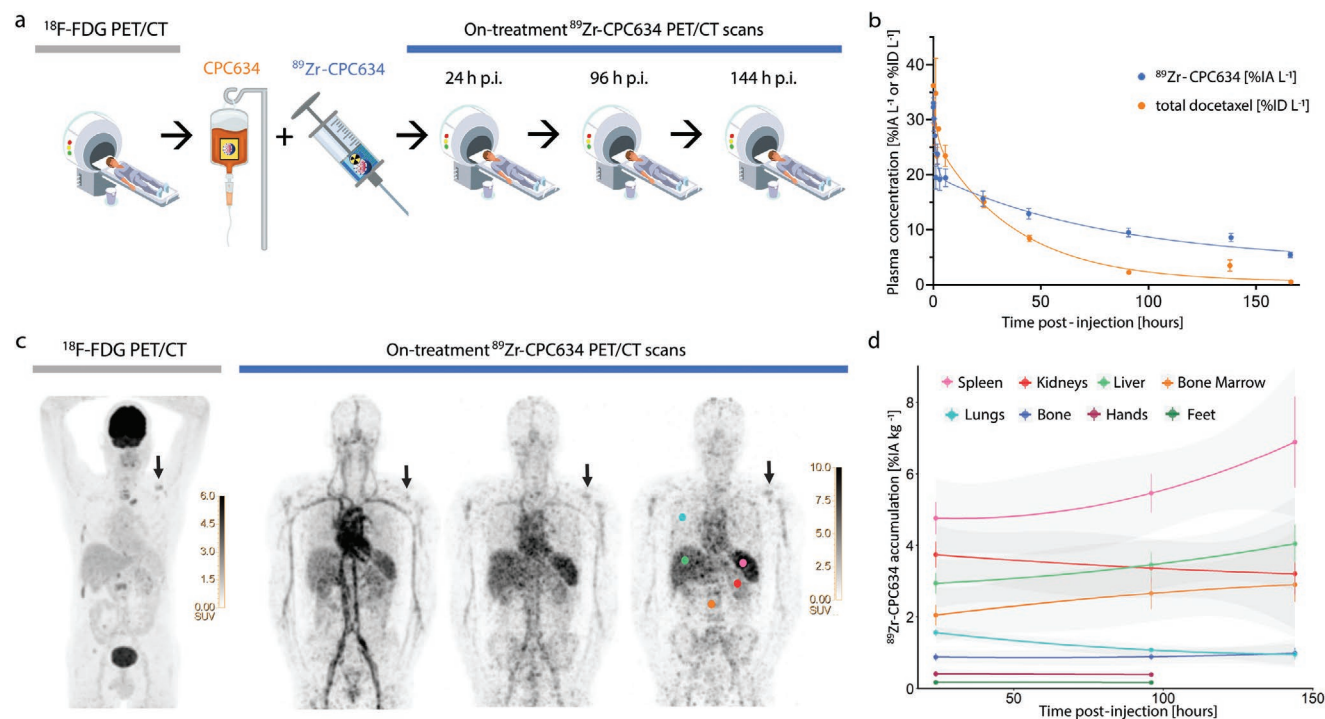


Figure 2. On-treatment imaging shows biodistribution of ^{89}Zr -CPC634. a) Schematic overview of on-treatment imaging setup. ^{18}F -FDG PET/CT scans were acquired at baseline. Within 2 h after the first therapeutic cycle of CPC634 (dose 60 mg m^{-2}) patients received ^{89}Zr -CPC634. PET/CT scans were made 24, 96, and 144 h post-injection. b) Plasma concentrations (mean \pm SD) of ^{89}Zr -CPC634 ($\% \text{IA L}^{-1}$) and total docetaxel ($\% \text{ID L}^{-1}$) show longevity of the nanoparticle in the plasma. c) MIP images of ^{18}F -FDG PET and on-treatment ^{89}Zr -CPC634 PET scans of a representative patient (patient 7) with adenocarcinoma of unknown primary. Black arrows indicate accumulation of ^{89}Zr -CPC634 in a bone metastasis. Tumor accumulation is further detailed in Figure 4. d) Quantification of accumulation of ^{89}Zr -CPC634 in major organs (spleen, kidneys, liver, bone marrow (excluding cortical bone), lungs, bone (= cortical bone)), and sites of possible skin toxicity (hands, feet). Points are mean values and the gray area represents the 95% CI. Organs were delineated manually, except for the bone (automatic CT threshold) and hands/feet (hands were fully delineated using a vacuum cushion and feet were fully delineated in a separate bed position, this procedure was not performed 144 h post-injection). Colored dots in (c) match organ colors in (d).

Similar to the preclinical experiments, after on-treatment administration of ^{89}Zr -CPC634, we analyzed two components in the plasma: the total docetaxel concentration ($\% \text{ID L}^{-1}$) and the radioactivity concentration ($\% \text{IA L}^{-1}$). Unexpectedly, we observed a rapid decline in radioactivity concentration in the first few hours after administration, which flattened between 6 and 24 h (Figure 2b), and importantly, was not observed in the preclinical study. The rapid drop in ^{89}Zr in plasma did not coincide with a decline in total docetaxel. The quality control (QC) pre-administration (performed with a 30 kDa molecular weight cut-off filter) demonstrated a purity of $>97\%$. After 24 h, radioactivity concentration continued to decrease with a more gradual pace, resulting in a decay-corrected circulation half-life of ^{89}Zr -CPC634 of $97.0 \pm 14.4 \text{ h}$. The ratio total docetaxel-to- ^{89}Zr decreased over time, corresponding with the anticipated release of docetaxel from the nanoparticles upon hydrolysis of the ester bond. Biodistribution analysis (Figure 2c,d and Figure S2, Supporting Information) showed accumulation of ^{89}Zr -CPC634 in spleen, liver, and bone marrow, known sites of nanoparticle uptake and elimination.^[18] The $\% \text{IA kg}^{-1}$ in hands and feet, known sites of toxicity,^[11] was low and stable over time. The $\% \text{IA kg}^{-1}$ in the kidneys decreased over time, indicating potential excretion of radioactivity via the kidneys, which was further characterized in the diagnostic dose

protocol. Findings on nanoparticle tumor accumulation are described below.

2.1.5. Diagnostic Dose Imaging Reveals a Similar PK Pattern and Biodistribution Profile of ^{89}Zr -CPC634

As confirmation of tumor accumulation prior to the start of treatment is highly desirable for patient stratification, we evaluated an 80-fold lower diagnostic dose of ^{89}Zr -CPC634 before the start of treatment (Figure 3a). We anticipated that the diagnostic dose, containing an absolute number of $1.8\text{--}3.7 \times 10^{14}$ nanoparticles, might be below the dose threshold, leading to rapid clearance of ^{89}Zr -CPC634 from the circulation, and therefore patients underwent an early time point of imaging. No AEs occurred that could be attributed to ^{89}Zr -CPC634. A PK pattern similar to the on-treatment dose was observed for both total docetaxel and radioactivity concentration in plasma, including a rapid decline of $\% \text{IA L}^{-1}$ in the first hours (Figure 3b and Figure S3, Supporting Information). The decay-corrected half-life of ^{89}Zr -CPC634 for the diagnostic dose was shorter than for the on-treatment dose (two-sided Student *t*-test, $p = 0.003$), but still demonstrated the longevity in the bloodstream with a mean half-life of $62.4 \pm 12.9 \text{ h}$ for the diagnostic dose. We did not

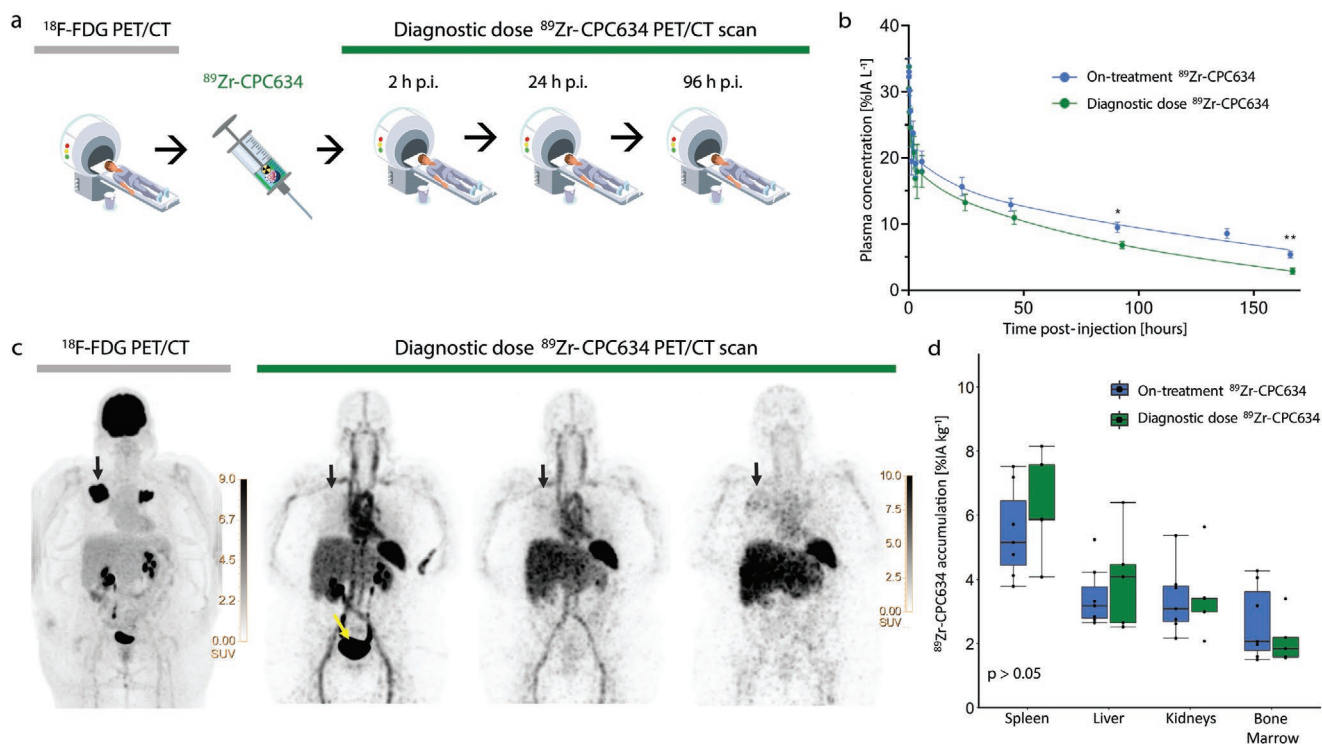


Figure 3. Imaging with a diagnostic dose results in similar PK and biodistribution. a) Schematic overview of imaging setup with a diagnostic dose: after baseline ^{18}F -FDG PET/CT patients directly received ^{89}Zr -CPC634 and PET/CT scans were made 2, 24, and 96 h post-injection. b) Plasma concentrations (mean \pm SD) of ^{89}Zr -CPC634 ($\%IA\ L^{-1}$) comparing on-treatment and diagnostic dose conditions. Two-sided student *t*-tests were performed: * $p < 0.05$, ** $p < 0.01$ ($N = 7$). c) MIP images of ^{18}F -FDG PET and diagnostic dose ^{89}Zr -CPC634 PET scans of a representative patient with metastasized endometrial cancer (patient 3). Black arrows indicate a metastasis in the right lung. Tumor accumulation is further detailed in Figure 4. Yellow arrow indicate urinary excretion 2 h post-injection. d) Comparison of major organs 96 h post-injection does not demonstrate significant difference in accumulation of ^{89}Zr -CPC634 (spleen, kidneys, liver, bone marrow) between on-treatment and diagnostic dose conditions. Kruskal–Wallis test was performed.

observe significant differences in accumulation of ^{89}Zr -CPC634 in major organs compared to the on-treatment dose (Figure 3d and Figure S4, Supporting Information). Information on radiation dosimetry is provided in Table S4 (Supporting Information).

In the diagnostic dose protocol, scans were made 2 h post-injection, revealing unexpected ^{89}Zr activity in the kidneys, ureters, and bladder at 2 h, but not at 24 h post-injection (Figure 3c), parallel to the rapid drop of ^{89}Zr in plasma we observed previously (Figure 2b). Therefore, in two subsequent patients, we collected urine during the first 24 h post-injection and found that 39.2% of the IA was rapidly excreted in the urine in the first few hours (Figure S5a, Supporting Information). Size fractionation revealed the majority of the activity (56%) had a molecular weight >30 kDa and 83% went through a 100 kDa molecular weight cut-off filter). Total docetaxel levels in urine were low. Adding an additional 100 kDa molecular weight cut-off filter to our QC, we could clear this fraction was at least in part already present pre-administration (Figure S5b, Supporting Information). To determine if the loss of the ^{89}Zr occurred in all patients in both on-treatment and diagnostic dose protocols, we checked the total image activity at 24 h post-injection (i.e., total $\%IA$ captured in the scan), and observed a loss of ^{89}Zr in all patients of $38.2\%IA \pm 2.8$, unrelated to renal function (no relation with plasma creatinine) (Figure S5c, Supporting Information). The fast elimination precluded contribution to tumor accumulation. Therefore, the $\%IA\ kg^{-1}$ accumulation values for

tumor lesions were corrected for the $\%IA$ excreted in urine for each patient individually. Biodistribution and plasma data are presented uncorrected. Additional corrected biodistribution analyses can be found in Figure S6 (Supporting Information).

2.1.6. Tumor Accumulation of ^{89}Zr -CPC634 Is Similar for Diagnostic Dose versus On-Treatment Dose

In total, 46 tumor lesions (in seven patients) were included in the on-treatment analysis and 32 in the diagnostic dose analysis, as identified on baseline ^{18}F -FDG PET and/or CT scan. Of these lesions, 21 out of 46 on-treatment (i.e., 46%; in seven patients) and 13 out of 32 diagnostic dose (i.e., 41%; in five patients) were visually positive for ^{89}Zr -CPC634 tumor accumulation (Figure 4a,b). Tumor accumulation was visible as early as 24 h post-injection (median $\%IA\ kg^{-1}$ 2.81; IQR 1.32–4.30) and increased significantly over time from 24 to 96 h post-injection (median $\%IA\ kg^{-1}$ 4.59; IQR 1.74–7.45; $p < 0.005$) and was stable from 96 to 144 h post-injection (median $\%IA\ kg^{-1}$ 6.00; IQR 2.37–9.63; $p = 0.18$). Importantly, there was no significant difference in $\%IA\ kg^{-1}$ between on-treatment and diagnostic dose (for 24 h post-injection: median 3.16 $\%IA\ kg^{-1}$; IQR 1.48–4.84 vs median 2.76 $\%IA\ kg^{-1}$; IQR 2.02–3.49, respectively, $p = 0.55$, and for 96 h post-injection median 4.94 $\%IA\ kg^{-1}$; IQR 2.18–7.70 vs 4.45 $\%IA\ kg^{-1}$; 1.68–7.22, respectively, $p = 0.91$). Tumor

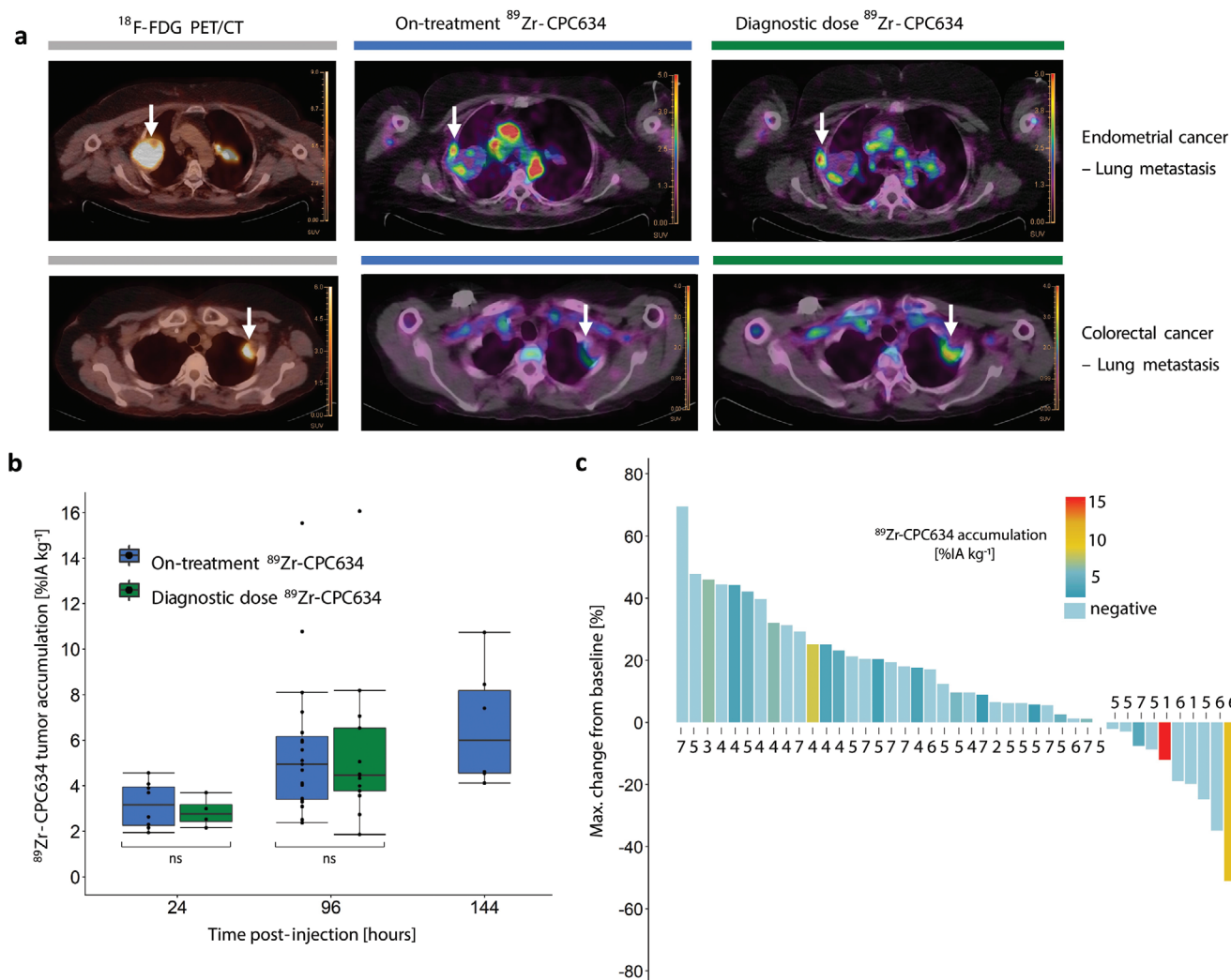


Figure 4. Visualization and quantification of tumor accumulation of ^{89}Zr -CPC634. a) Two representative examples of tumor accumulation (upper panel patient 3, lower panel patient 4) at 96 h post-injection showing both on-treatment and diagnostic dose imaging, arrows indicate tumor lesions. b) Quantitative analyses of all visually positive tumors at several time points corrected for urinary excretion ($N = 21$). Individual tumors are indicated by black dots. Results of Mann–Whitney U test are shown ns = $p > 0.05$. c) Waterfall plot of all tumor lesions 96 h post-injection on-treatment with the %IA kg⁻¹, corrected for urinary excretion, depicted as a gradient and the bar representing the maximum percentage change from baseline. Each bar represents a single tumor lesion and patient numbers (corresponding to Table 1) are indicated below or on top of the bar. Note that there are multiple bars per patient in most cases.

accumulation was heterogeneous between and within subjects (Figure S7, Supporting Information), as well as within individual tumor lesions (Figure 4a). There was no correlation between FDG SUV_{max} and ^{89}Zr -CPC634 tumor accumulation (diagnostic dose: Spearman's rank, $r = 0.25$, $p = 0.4$; on-treatment: Spearman's rank, $r = 0.055$, $p = 0.82$). ^{89}Zr -CPC634 did not accumulate in necrotic areas identified on CT or ^{18}F -FDG PET.

Using these data to estimate the intratumoral concentration of nanoparticle-entrapped docetaxel, we first calculated the ratio between total docetaxel and radioactivity in plasma (corrected for urinary excretion), which represents the fraction of nanoparticles still containing entrapped docetaxel (Figure S8, Supporting Information). Assuming a similar ratio in tumors and using the %IA kg⁻¹ that had accumulated in tumors, the concentration

of nanoparticle-entrapped docetaxel can be estimated, and was found to be median 2.29 (IQR 2.00–3.23) and 0.83 (IQR 0.48–1.21) ng mg⁻¹ after 24 and 96 h post-injection, respectively.

2.1.7. Initial Results on Response Prediction with ^{89}Zr -CPC634

In this heavily pretreated cohort of patients, three out of seven patients (i.e., 43%) achieved stable disease and four showed progressive disease at first evaluation. Two of these patients (subjects 1 and 6) experienced a decrease in tumor marker (CA125/CA15.3). One of them also had a noticeable decrease in target lesions but did not reach a partial response (subject 6; 28% decrease in diameter of target lesions). At the per-patient level, no association was found between ^{89}Zr -CPC634 tumor

Table 1. Tumor accumulation of ^{89}Zr -CPC634 per patient. All patients are indicated with tumor type, number of positive and total lesions and best response is shown.

Subject no.	Tumor type	Positive lesions on-treatment/no. [%]	Positive lesions diagnostic dose/no. [%]	Best response
1	Ovarian carcinoma	1/2 [50]	1/2 [50]	SD
2	Esophageal carcinoma	0/1	0/1	PD
3	Endometrial carcinoma	2/2 [100]	2/2 [100]	PD ^{a)}
4	Colorectal carcinoma	6/10 [60]	5/10 [50]	PD
5	Myoepithelial carcinoma	6/17 [35]	5/17 [29]	SD ^{b)}
6	Breast cancer	1/5 [20]	NA	SD
7	Adenocarcinoma of unknown primary	5/9 [56]	NA	PD
Total		21/46 [46]	13/32 [41]	

^{a)}For patient 3 one lesion was irradiated and not included in FU size measurement; ^{b)}For patient 5 two lesions were not included in FU size measurements for these were only recognizable on ^{18}F -FDG PET and not on FU CT-scans.

accumulation and therapeutic response (Table 1 and Figure S9, Supporting Information). However, for individual lesions, we observed the highest uptake of ^{89}Zr -CPC634 in two lesions with 12% and 51% decrease in diameter (Figure 4c).

3. Discussion

In this study, we present a new clinical tool for the visualization and quantification of polymeric nanoparticle tumor targeting via noninvasive PET/CT imaging with a low diagnostic dose of ^{89}Zr -CPC634. The tumor accumulation of nanoparticles can be highly variable within and between patients, explaining—at least in part—why nanomedicine treatment often results in a relatively disappointing clinical efficacy.^[6,19] Quantitative clinical tools are much needed to advance our understanding and ultimately aid in patient selection.

To be able to select patients before starting treatment, one would ideally use a low dose, to protect patients from treatment with ineffective but potentially toxic dosages. In this regard, it is important to keep in mind that the core-crosslinked polymeric micelle delivery platform used is well-tolerated and does not elicit ancillary effects.^[20] We used a diagnostic dose of CPC634 containing 1–2 mg total docetaxel, which is equivalent to an absolute number of $\approx 1.8\text{--}3.7 \times 10^{14}$ nanoparticles per patient. We demonstrated that with this diagnostic dose, we could achieve adequate visualization and quantification of ^{89}Zr -CPC634 in human solid tumors, with a similar profile as the on-treatment dose which contained $1.8\text{--}2.2 \times 10^{16}$ nanoparticles per patient, and more importantly, without causing any adverse effects. The exact nanoparticle dose threshold in humans has not been established, but was recently estimated to be around 1.5×10^{15} based on extrapolation from preclinical data from liposomal nanoparticles.^[17] Our data suggest that this threshold might be ten-fold lower in practice, and/or that a lower threshold applies to long-circulating nanoparticles which are characterized by the absence of opsonization and protein corona formation.^[9]

From this first-in-human imaging study with ^{89}Zr -labeled polymeric nanoparticles, lessons were learned that without imaging would have gone unnoticed. In contrast to the

preclinical study, in the clinical part we observed rapid excretion of ^{89}Zr via the urine, without a corresponding decline in total docetaxel plasma levels. This pointed to a ^{89}Zr -labeled byproduct unrelated to intact ^{89}Zr -CPC634. Theoretically, based on the chemical composition, three byproducts were considered: 1) free ^{89}Zr , 2) free ^{89}Zr -DFO, and 3) ^{89}Zr -labeled DFO-containing polymeric aggregates, where (1) was considered highly unlikely considering ^{89}Zr is a bone seeking mineral and no signs of bone uptake were observed. Analysis of the byproduct in the urine using molecular weight cut-off filters, indicated the impurity was most likely the third postulated byproduct, ^{89}Zr -labeled DFO-containing polymeric aggregates. Between the preclinical and the clinical batch, the manufacturing process of DFO-CPC634 was scaled up. Despite careful synthesis method transfer, analytical method validation and thorough nanoparticle purification by tangential flow filtration, in hindsight a critical quality attribute, namely size fractionation, has been lacking. In addition, the presence of ^{89}Zr -labeled DFO-containing polymeric aggregates was neither identified in the quality controls used for clinical approval of ^{89}Zr -CPC634 administration, for which the 30 kDa molecular weight cut-off filter assay indicated >97% radiochemical purity. This quality control had been validated in advance for being capable of separating ^{89}Zr -CPC634 from free ^{89}Zr and ^{89}Zr -DFO, but not from impurities with a higher molecular weight like the ^{89}Zr -labeled DFO-containing polymeric aggregates. As a result, size fractionation has now been introduced in nanoparticle production and characterization as to monitor the presence of potential residual polymeric aggregates. It is important to note that the residual polymeric aggregates do not pose any safety concerns due to their rapid urinary excretion. Furthermore, because docetaxel is conjugated to the crosslinker and introduced into the nanoparticles during the core-crosslinking process, the therapeutic performance of the nanomedicine formulation is not compromised by the presence of polymeric aggregates. Further development of ^{89}Zr -CPC634 should include confirmation of our results and elimination of the impurity in DFO-CPC634 batch via the simple size fractionation. However, the amount of radioactivity excreted in urine was very similar between patients ($38.2 \pm 2.8\%$), and tumor accumulation was corrected

for the urinary excretion, thus the impurity is not expected to influence findings on tumor accumulation.

By measuring both total docetaxel and ^{89}Zr -CPC634 in plasma, we were able to measure both the drug and its nanocarrier in the systemic circulation. We demonstrated the longevity of ^{89}Zr -CPC634 nanoparticles in the bloodstream (decay-corrected half-life of 970 ± 14.4 h) and the slow release of the entrapped docetaxel. Extrapolating the same release-kinetics to the tumor, we estimated that the amount of docetaxel still entrapped in CPC634 in tumors was median 2.29 (IQR 2.00–3.23) and 0.83 (IQR 0.48–1.21) ng mg^{-1} after 24 and 96 h post-injection respectively, based on an administered dose of 60 mg m^{-2} . Presumably, once docetaxel is released from the nanoparticle, most of it will remain in the tumor microenvironment because of the lack of lymphatic drainage, and this will result in a local buildup of docetaxel over time. This hypothesis is supported by the results from the previously performed CriTax study, in which intratumoral total docetaxel concentrations were higher—3.70, 95% CI: 2.56–4.55 ng mg^{-1} and 4.54, 95% CI: 2.16–9.56 ng mg^{-1} in tumor biopsies at 24 and 96 h, respectively—after i.v. administration of 75 mg m^{-2} CPC634.^[12]

While the importance of patient selection for cancer nanomedicine has been widely acknowledged, hardly any clinical study has thus far focused on creating diagnostic tools for implementation in clinical practice. Only one other nanomedicine formulation has been studied using PET/CT imaging, but this was liposome-based and only on-treatment imaging was performed.^[21] The tested ^{64}Cu -labeled doxorubicin-loaded liposomes were surface-modified with an anti-HER2 antibody, and were evaluated in patients with metastatic breast cancer. These targeted liposomal nanomedicines demonstrated a slightly higher tumor accumulation (4.0 %IA kg^{-1} 48 h post-injection) as compared to ^{89}Zr -CPC634, which can likely be partially explained by the active targeting approach. An additional explanation may be that liver lesions were included in this analysis, which is disregarded in the current study because of the high background accumulation in healthy liver tissue due to Kupffer cell uptake of nanoparticles. An alternative to theranostic PET/CT is visualizing and quantifying nanoparticle tumor accumulation via companion diagnostics. A pioneering proof-of-concept study in this regard was published by Ramanathan and colleagues, showing that assessment of iron oxide nanoparticle uptake in tumors via MRI correlates with anti-tumor response to liposomal irinotecan.^[22]

As expected, we observed relatively high inter- and inpatient heterogeneity in the tumor accumulation of ^{89}Zr -CPC634. Factors underlying this heterogeneity are believed to be mostly related to the tumor vasculature and stroma composition.^[15,18] As a surrogate measure for perfusion, we hypothesized that areas with ^{18}F -FDG uptake were, at least to some extent, vascularized and might therefore correspond to the areas of nanoparticle uptake. However, we found that within regions of high ^{18}F -FDG uptake, only restricted areas (hotspots) showed strong accumulation of ^{89}Zr -CPC634. Presumably these hotspots harbor ideal conditions for extravasation and retention of nanoparticles, and are able to provide sustained release of docetaxel to the surrounding tumor cells. Further enhancement of nanoparticle accumulation might be achieved by co-administering CPC634 together with vascular and microenvironment

modulators, such as losartan.^[23] The efficacy of such strategies can be non-invasively visualized and quantified (and their use in patients tailored) via PET/CT-based imaging of nanoparticle tumor accumulation.

In this heavily pretreated cohort of seven patients, which included various cancer types and sites of metastases, we found high tumor accumulation in two lesions that also had a corresponding decrease in diameter. However, in the same patients other lesions that decreased in size were visually negative for nanoparticle accumulation. Collecting information on a per-lesion basis and including the number of negatively scored lesions is key in understanding the complex pattern of inpatient heterogeneity and how this might relate to responses at the patient level. In this way, defining a reliable strategy for patient stratification with ^{89}Zr -CPC634 is certainly achievable, but was ultimately not possible in the current clinical study. Further optimization is needed in a homogenous (and less heavily pretreated) patient population, ideally with a single solid tumor type, and preferably one with a good response rate for docetaxel. Additionally, a combination arm in which nanoparticle therapy is combined with a vascular modulator could be added, to explore the possible potentiation of tumor accumulation.

4. Conclusion

In summary, we show that a low diagnostic dose of ^{89}Zr -CPC634 enables visualization and quantification of nanoparticle accumulation in human solid tumors by means of PET/CT. This may ultimately serve as a tool for patient stratification in case of treatment with CPC634 (and other cancer nanomedicines). Further prospective clinical trials are needed to validate this tool and achieve clinical implementation.

5. Experimental Section

Patient Selection: Patients with advanced solid tumors, not amendable to standard treatment options, were eligible for this study. Other inclusion criteria were: measurable disease according to RECIST 1.1,^[24] at least one measurable lesion of ≥ 2 cm outside of the liver, performance status of 0–1 according to Eastern Cooperative Oncology Group, adequate hepatic, renal, and bone marrow function, life expectancy of at least 12 weeks, and age ≥ 18 years. Exclusion criteria included: any other anticancer therapy or treatment with another investigational drug within the last four weeks, active or symptomatic brain metastases, current invasive malignancies at other sites, major surgical procedure within the last 28 d, uncontrolled hypertension, significant cardiovascular disease, neuropathy grade ≥ 2 , ongoing toxicities grade ≥ 2 from previous anticancer therapies, hypersensitivity to taxanes, a history of skin toxicity as a result of prior treatment with taxanes and any active skin condition putting the patient at risk of developing skin toxicity.

Study Design: This clinical trial was conducted at Amsterdam UMC, location VUmc. All patients provided written informed consent. This study was approved by the Medical Ethics Review Committee of the VU University medical center (under registration number 2017.591) and conducted following the International Conference on Harmonization guidelines, and in accordance with Good Clinical Practice and the Declaration of Helsinki.^[25] This trial was registered at www.clinicaltrials.gov (NCT03712423), first submitted October 3, 2017, and as a phase-I trial in the EudraCT database (2017-0034664-12), first listed October 23, 2017.

As part of the study protocol baseline ^{18}F -FDG PET/CT scans were performed according to the EANM guidelines 2.0.^[26] Whole-body images were acquired 60 min after i.v. administration of 2.5 MBq kg^{-1} [^{18}F]-FDG. The baseline ^{18}F -FDG PET/CT scan was performed within two weeks before the first ^{89}Zr -CPC634 injection. In the diagnostic dose imaging setup, patients received a diagnostic dose of ^{89}Zr -CPC634 (37 MBq, 1–2 mg docetaxel) as an i.v. infusion over 10 min. Whole-body PET/CT scans were obtained at 1.6 (range 1.4–2.2), 24.4 (range 22.7–25.9), and 92.5 (range 90.4–97.5) h post-injection. In the on-treatment imaging setup, patients were treated with their first therapeutic cycle of CPC634 at the recommended phase-II dose of 60 mg m^{-2} . Within 2 h after the end of CPC634 infusion, patients received ^{89}Zr -CPC634 (37 MBq, 1–2 mg docetaxel) as an i.v. infusion over 10 min. Whole-body PET/CT scans were obtained at 23.8 (range 21.1–25.2), 90.1 (range 88.0–91.0), and 137.5 (range 137.2–137.8) h post-injection. Patients who participated in both the diagnostic dose and on-treatment imaging protocols, started with the first tracer administration in the diagnostic dose and continued two weeks later with the second tracer administration in the on-treatment protocol. For these patients the baseline ^{18}F -FDG PET was not repeated in between. After completing the imaging procedures, patients continued to receive three-weekly administrations of CPC634 containing 60 mg m^{-2} docetaxel until disease progression or unacceptable toxicities occurred. CPC634 was provided by Cristal Therapeutics (Maastricht, The Netherlands) and was administered as an i.v. solution over 1 h with premedication consisting of 8 mg oral dexamethasone (at 12, 3, and 1 h before infusion). Diagnostic CT scans, performed at baseline and after every second therapy cycle, were evaluated according to RECIST 1.1.^[24] AEs were classified according to Common Terminology Criteria for Adverse Events (version 4.3) and recorded at every visit and until one month after end of treatment. From two patients urine was collected for 24 h after administration of ^{89}Zr -CPC634 (on-treatment).

Radioactivity and Total Docetaxel Analysis in Plasma and Urine: Venous blood samples were drawn at various time points following injection of ^{89}Zr -CPC634. Radioactivity concentration in blood, plasma, and urine was measured in a cross-calibrated well counter.^[27] Plasma and urine samples for total docetaxel measurements were stored at $-80\text{ }^{\circ}\text{C}$ and after ≥ 28 d of decay shipped and subsequently measured at the lab of Translational Pharmacology (Rotterdam, the Netherlands) using a validated liquid chromatographic method.^[28] PK analysis was performed using Phoenix WinNonlin Version 7 (Certara USA, Inc., Princeton, NJ).

Manufacturing of CPC634 and DFO-Functionalized CPC634: The manufacturing scheme of DFO-functionalized CPC634 (DFO-CPC634) is described in Figure S10 (Supporting Information). While solely CriPec block copolymer [methacrylated mPEG₅₀₀₀-*b*-p(HPMAMLaC₁Lac₂)] was used to manufacture CPC634,^[7] a mixture of CriPec block copolymer (99 mol%) and azide-functionalized CriPec block copolymer [1 mol%, methacrylated azide-PEG₅₀₀₀-*b*-p(HPMAMLaC₁Lac₂)] of the same molecular mass, comonomer ratio and methacrylation extent (mol%) were used to synthesize azide-functionalized CPC634 essentially following the same manufacturing protocol.^[29] The generated azide-functionalized CPC634 were purified and concentrated to 100 mg mL^{-1} polymer equivalent by means of Tangential Flow Filtration (TFF, 100 kDa mPES module, Spectrumbioscience). To generate DFO-CPC634, an excess (20 equivalents relative to azide) of BCN-desferal (BCN-DFO, see synthesis details in Figure S11, Supporting Information) was conjugated to azide-functionalized CPC634 via irreversible copper-free click chemistry, followed by purification via TFF, yielding DFO-CPC634 exhibiting the same physicochemical characteristics as CPC634 (Table S1 and Figure S1, Supporting Information). The manufactured DFO-CPC634 was diluted to 3.7 mg mL^{-1} docetaxel equivalent (32 mg mL^{-1} polymer equivalent) in the same vehicle (20 $\times 10^{-3}$ M ammonium acetate pH 5 buffer containing 130 $\times 10^{-3}$ M NaCl) and stored at $< -60\text{ }^{\circ}\text{C}$ till radiolabeling production. After in-house synthesis and analytical method development, all procedures were transferred to an experienced party who performed all synthesis steps (including synthesis of intermediates) and final analytical characterization of CPC634 and DFO-CPC634 under current Good Manufacturing Practice (cGMP) conditions. GMP-complaint Fill and Finish into zenith vials was conducted by another experienced party

and the generated CPC634 and DFO-CPC634 drug products were stored at $< -60\text{ }^{\circ}\text{C}$ under GMP conditions.

Preparation and Analysis of ^{89}Zr -CPC634 for (Pre)clinical Use: Details on radiolabeling, quality control testing, and formulation as well as preclinical experiments can be found in the Supporting Information. For clinical use, DFO-CPC634 was radiolabeled with ^{89}Zr according to cGMP standards. In short, DFO-CPC634 (32 mg mL^{-1}), was first rebuffed using a pyrogen-free PD10 column (GE Healthcare) to 20 $\times 10^{-3}$ M sodium acetate, 130 $\times 10^{-3}$ M NaCl pH 4.5–5.5. To 150 μL 1 M oxalic acid containing the required amount of ^{89}Zr (≈ 150 MBq) were added 68 μL 2 M Na_2CO_3 . After 3 min 0.5 mL 0.5 M HEPES and 0.5–1 mL DFO-CPC634 (22–24 mg mL^{-1} polymer equivalent) were added and reacted for 120 min, followed by purification on two pyrogen-free PD10 columns. The final product was eluted in 20 $\times 10^{-3}$ M ammonium acetate and 130 $\times 10^{-3}$ M NaCl buffer pH 4.5–5.5. The radiochemical purity was 97.5 \pm 1.5% as assessed by 30 kDa molecular weight cut-off filter, able to distinguish ^{89}Zr -CPC634 (molecular weight ≈ 22000 kDa) from free ^{89}Zr (0.09 kDa) and free ^{89}Zr -DFO (0.91 kDa).^[30] The endotoxin content was < 0.2 EU mL^{-1} and the pH was 5.3 \pm 0.1 and met the reset requirements for injection. See the Supporting Information for a detailed description. The final ^{89}Zr -CPC634 tracer contained 8.4 mg DFO-CPC634 (equivalent 1–2 mg of docetaxel, molecular weight 22 kDa per polymer).

^{89}Zr -CPC634 PET/CT Scan Acquisition and Analysis: Scan Acquisition: Following low dose CT-scan for attenuation correction, whole-body PET scans were acquired from head to mid-thigh with a scan duration of 5 min. per bed position, resulting in a total scan duration of ≈ 60 min. Four patients were scanned with the hands in a vacuum cushion and with an additional bed position for imaging of the feet. All PET/CT scans were performed either on an Ingenuity or Vereos digital PET/CT (both from Philips Medical Systems, Best, The Netherlands).

Analysis of Tumor Accumulation of ^{89}Zr -CPC634: PET image analysis was performed using the in-house developed software ACCURATE.^[31] For quantification of tumors, only lesions ≥ 2 cm in diameter were included to rule out partial volume effects.^[32] Furthermore, tumors located in the liver (because of high background due to nanoparticle metabolism in the liver) or without a clear delineation on either ^{18}F -FDG PET or diagnostic CT/MRI scan were excluded from analysis. Accumulation of ^{89}Zr -CPC634 in tumors was analyzed using a previously described standardized manual procedure for tumor segmentation.^[33] In short, lesions were scored by an experienced nuclear medicine physician (GZ) who was initially blinded for ^{18}F -FDG PET and diagnostic CT/MRI images. Lesions on the ^{89}Zr -CPC634 PET were scored as visually positive when focal uptake exceeded local background. Thereafter, the ^{18}F -FDG PET and diagnostic CT or MRI were used as reference to score the initially unevaluated lesions. For positive tumors, volumes of interest (VOI) were delineated on the PET image by the physician-researcher (IM), and then verified by GZ. Tumor accumulation is calculated assuming 1 L corresponds to 1 kg, and is reported as % injected activity per kilogram (%IA kg^{-1} , based on peak activity concentration), as this outcome has an excellent interobserver reproducibility.^[33] Additionally, SUV_{peak} values are reported in Figure S11 (Supporting Information).

Correction for Urinary Excretion of ^{89}Zr -Labeled Byproduct: The calculated %IA kg^{-1} per tumor was corrected for individual urinary excretion as follows: from two patients urinary excretion was measured over 24 h (41.4 and 37.0%IA), and for these two patients the %IA was corrected for this loss. It was assumed that the total activity at the scan 24 h after injection (53.1 and 52.9%IA), as measured by PET from head to mid-thigh, together with the urinary excretion represented the total %IA (92.2). The remaining 7.8%IA is most probably present in the lower extremities, which were not included in the PET scanning trajectory. Consequently, for patients who did not undergo 24 h urine collection, the urinary excretion was then estimated to be 92.2% minus the total image activity at 24 h post-injection, resulting in an estimated mean urinary excretion of 38.2% \pm 2.8.

Analysis of Biodistribution of ^{89}Zr -CPC634: To assess biodistribution, organs of interest were delineated either manually (lungs, spleen, liver, kidneys, bone marrow, hands) or automatically (bone, feet) using

the in-house developed BIODISTRIBUTION tool (developed in IDL version 8.4).

Statistical Analysis: Statistical analyses were performed in R software version 3.6.3 for Windows using the Kruskal–Wallis test for nonparametric data and comparison between multiple groups, followed if significant by a Mann–Whitney U test corrected for multiple testing (Figures 3d and 4b; Figures S4 and S9, Supporting Information). For patients participating in both on-treatment and diagnostic dose protocols, additional paired analyses (paired Wilcoxon signed rank test) on tumor lesions was performed (Figure S12, Supporting Information). For correlation analysis Spearman's rank was used. Nonparametric data are reported as median (IQR). For parametric data, a one-way ANOVA (Figure S1, Supporting Information) or two-tailed unpaired *t*-tests (Figure 3b and Figure S3, Supporting Information) were performed. Parametric data were presented as mean ± SD. A *p*-value of <0.05 was considered as statistically significant. No preprocessing was applied. No formal sample size was calculated. After inclusion of seven patients (on-treatment *N* = 7, diagnostic dose *N* = 5) data analysis showed consistent results and inclusion was stopped.

Supporting Information

Supporting Information is available from the Wiley Online Library or from the author.

Acknowledgements

The authors like to acknowledge the significant contributions of Jimmy Weterings on the design and actual synthesis of BCN-desferal and Rob Hanssen for all (pre)clinical study support, both employees of Cristal Therapeutics at the time of study execution. This study was supported by Health Holland and financial contributions of Cristal Therapeutics (CT). CT participated in the design, study conduct, analysis, and interpretation of the data and approval of this manuscript.

Conflict of Interest

C.R. and Q.H. are employees of Cristal Therapeutics. C.W.M. and R.M. received research funding from Cristal Therapeutics. The authors declare that they have no other competing interests.

Data Availability Statement

The data that support the findings of this study are available from the corresponding author upon reasonable request.

Keywords

⁸⁹Zr, cancer, docetaxel, nanomedicines, PET/CT imaging, polymeric nanoparticles, solid tumors

Received: January 31, 2022

Revised: April 8, 2022

Published online: April 25, 2022

- [1] a) S. J. Clarke, L. P. Rivory, *Clin. Pharmacokinet.* **1999**, *36*, 99; b) P. C. Barata, A. O. Sartor, *Cancer* **2019**, *125*, 1777.
[2] a) A. Argiris, M. Ghebremichael, J. Gilbert, J. W. Lee, K. Sachidanandam, J. M. Kolesar, B. Burtness, A. A. Forastiere, *J. Clin. Oncol.* **2013**, *31*, 1405; b) J. A. Sparano, *Clin. Breast Cancer*

- 2000**, *1*, 32; c) D. R. Berthold, G. R. Pond, F. Soban, R. de Wit, M. Eisenberger, I. F. Tannock, *J. Clin. Oncol.* **2008**, *26*, 242; d) W. Schuette, S. Nagel, T. Blankenburg, G. Lautenschlaeger, K. Hans, E. W. Schmidt, I. Dittrich, H. Schweisfurth, L. F. von Weikersthal, A. Raghavachar, A. Reissig, M. Serke, *J. Clin. Oncol.* **2005**, *23*, 8389.
[3] A. J. Nieuweboer, E. S. de Morree, A. J. de Graan, A. Sparreboom, R. de Wit, R. H. Mathijssen, *Cancer Treat. Rev.* **2015**, *41*, 605.
[4] A. A. van der Veldt, M. Lubberink, R. H. Mathijssen, W. J. Loos, G. J. Herder, H. N. Greuter, E. F. Comans, H. B. Rutten, J. Eriksson, A. D. Windhorst, N. H. Hendrikse, P. E. Postmus, E. F. Smit, A. A. Lammertsma, *Clin. Cancer Res.* **2013**, *19*, 4163.
[5] M. Y. Ho, J. R. Mackey, *Cancer Manage. Res.* **2014**, *6*, 253.
[6] R. A. G. Van Eerden, R. H. Mathijssen, S. L. W. Koolen, *Int. J. Nanomed.* **2020**, *15*, 8151.
[7] Q. Hu, C. J. Rijcken, R. Bansal, W. E. Hennink, G. Storm, J. Prakash, *Biomaterials* **2015**, *53*, 370.
[8] Q. Hu, C. J. Rijcken, E. van Gaal, P. Brundel, H. Kostkova, T. Etrych, B. Weber, M. Barz, F. Kiessling, J. Prakash, G. Storm, W. E. Hennink, T. Lammers, *J. Controlled Release* **2016**, *244*, 314.
[9] I. Alberg, S. Kramer, M. Schinnerer, Q. Hu, C. Seidl, C. Leps, N. Drude, D. Mockel, C. Rijcken, T. Lammers, M. Diken, M. Maskos, S. Morsbach, K. Landfester, S. Tenzer, M. Barz, R. Zentel, *Small* **2020**, *16*, e1907574.
[10] Y. Matsumura, H. Maeda, *Cancer Res.* **1986**, *46*, 6387.
[11] F. Atrafi, H. Dumez, R. H. J. Mathijssen, C. W. Menke van der Houven van Oordt, C. J. F. Rijcken, R. Hanssen, F. Eskens, P. Schoffski, *J. Controlled Release* **2020**, *325*, 191.
[12] F. Atrafi, R. A. G. van Eerden, M. A. M. van Hylckama Vlieg, E. Oomen-de Hoop, P. de Bruijn, M. P. Lolkema, A. Moelker, C. J. Rijcken, R. Hanssen, A. Sparreboom, F. Eskens, R. H. J. Mathijssen, S. L. W. Koolen, *Clin. Cancer Res.* **2020**, *26*, 3537.
[13] a) G. P. Stathopoulos, D. Antoniou, J. Dimitroulis, J. Stathopoulos, K. Marosis, P. Michalopoulou, *Cancer Chemother. Pharmacol.* **2011**, *68*, 945; b) G. Delgado, R. K. Potkul, J. A. Treat, G. S. Lewandowski, J. F. Barter, D. Forst, A. Rahman, *Am. J. Obstet. Gynecol.* **1989**, *160*, 812; c) W. J. Gradishar, S. Tjulandin, N. Davidson, H. Shaw, N. Desai, P. Bhar, M. Hawkins, J. O'Shaughnessy, *J. Clin. Oncol.* **2005**, *23*, 7794.
[14] a) S. Sindhwan, A. M. Syed, J. Ngai, B. R. Kingston, L. Maiorino, J. Rothschild, P. MacMillan, Y. Zhang, N. U. Rajesh, T. Hoang, J. L. Y. Wu, S. Wilhelm, A. Zilman, S. Gadde, A. Sulaiman, B. Ouyang, Z. Lin, L. Wang, M. Egeblad, W. C. W. Chan, *Nat. Mater.* **2020**, *19*, 566; b) F. Danhier, *J. Controlled Release* **2016**, *244*, 108; c) S. K. Golombek, J. N. May, B. Theek, L. Appold, N. Drude, F. Kiessling, T. Lammers, *Adv. Drug Delivery Rev.* **2018**, *130*, 17.
[15] J. Fang, W. Islam, H. Maeda, *Adv. Drug Delivery Rev.* **2020**.
[16] G. van Dongen, W. Beaino, A. D. Windhorst, G. J. C. Zwezerijnen, D. E. Oprea-Lager, N. H. Hendrikse, C. van Kuijk, R. Boellaard, M. C. Huisman, D. J. Vugts, *J. Nucl. Med.* **2021**, *62*, 438.
[17] B. Ouyang, W. Poon, Y. N. Zhang, Z. P. Lin, B. R. Kingston, A. J. Tavares, Y. Zhang, J. Chen, M. S. Valic, A. M. Syed, P. MacMillan, J. Couture-Senecal, G. Zheng, W. C. W. Chan, *Nat. Mater.* **2020**.
[18] M. J. Ernsting, M. Murakami, A. Roy, S. D. Li, *J. Controlled Release* **2013**, *172*, 782.
[19] R. van der Meel, E. Sulheim, Y. Shi, F. Kiessling, W. J. M. Mulder, T. Lammers, *Nat. Nanotechnol.* **2019**, *14*, 1007.
[20] a) E. P. Stater, A. Y. Sonay, C. Hart, J. Grimm, *Nat. Nanotechnol.* **2021**, *16*, 1180; b) M. Talelli, M. Iman, A. K. Varkouhi, C. J. Rijcken, R. M. Schifferlers, T. Etrych, K. Ulbrich, C. F. van Nostrum, T. Lammers, G. Storm, W. E. Hennink, *Biomaterials* **2010**, *31*, 7797.
[21] H. Lee, A. F. Shields, B. A. Siegel, K. D. Miller, I. Krop, C. X. Ma, P. M. LoRusso, P. N. Munster, K. Campbell, D. F. Gaddy,

- S. C. Leonard, E. Geretti, S. J. Blocker, D. B. Kirpotin, V. Moyo, T. J. Wickham, B. S. Hendriks, *Clin. Cancer Res.* **2017**, *23*, 4190.
- [22] R. K. Ramanathan, R. L. Korn, N. Raghunand, J. C. Sachdev, R. G. Newbold, G. Jameson, G. J. Fetterly, J. Prey, S. G. Klinz, J. Kim, J. Cain, B. S. Hendriks, D. C. Drummond, E. Bayever, J. B. Fitzgerald, *Clin. Cancer Res.* **2017**, *23*, 3638.
- [23] J. E. Murphy, J. Y. Wo, D. P. Ryan, J. W. Clark, W. Jiang, B. Y. Yeap, L. C. Drapek, L. Ly, C. V. Baglini, L. S. Blaszkowsky, C. R. Ferrone, A. R. Parikh, C. D. Weekes, R. D. Nipp, E. L. Kwak, J. N. Allen, R. B. Corcoran, D. T. Ting, J. E. Faris, A. X. Zhu, L. Goyal, D. L. Berger, M. Qadan, K. D. Lillemoe, N. Talele, R. K. Jain, T. F. DeLaney, D. G. Duda, Y. Boucher, C. Fernandez-Del Castillo, et al, *JAMA Oncol.* **2019**, *5*, 1020.
- [24] E. A. Eisenhauer, P. Therasse, J. Bogaerts, L. H. Schwartz, D. Sargent, R. Ford, J. Dancey, S. Arbuck, S. Gwyther, M. Mooney, L. Rubinstein, L. Shankar, L. Dodd, R. Kaplan, D. Lacombe, J. Verweij, *Eur. J. Cancer* **2009**, *45*, 228.
- [25] A. World Medical, *JAMA, J. Am. Med. Assoc.* **2013**, *310*, 2191.
- [26] R. Boellaard, R. Delgado-Bolton, W. J. Oyen, F. Giammarile, K. Tatsch, W. Eschner, F. J. Verzijlbergen, S. F. Barrington, L. C. Pike, W. A. Weber, S. Stroobants, D. Delbeke, K. J. Donohoe, S. Holbrook, M. M. Graham, G. Testanera, O. S. Hoekstra, J. Zijlstra, E. Visser, C. J. Hoekstra, J. Pruim, A. Willemsen, B. Arends, J. Kotzerke, A. Bockisch, T. Beyer, A. Chiti, B. J. Krause, M. European Association of Nuclear, *Eur. J. Nucl. Med. Mol. Imaging* **2015**, *42*, 328.
- [27] H. N. Greuter, P. L. van Ophemert, G. Luurtsema, E. J. Franssen, R. Boellaard, A. A. Lammertsma, *J. Nucl. Med. Technol.* **2004**, *32*, 28.
- [28] C. L. Braal, P. de Bruijn, F. Atrafi, M. van Geijn, C. J. F. Rijcken, R. H. J. Mathijssen, S. L. W. Koolen, *J. Pharm. Biomed. Anal.* **2018**, *161*, 168.
- [29] I. Biancacci, Q. Sun, D. Mockel, F. Gremse, S. Rosenhain, F. Kiessling, M. Bartneck, Q. Hu, M. Thewissen, G. Storm, W. E. Hennink, Y. Shi, C. J. F. Rijcken, T. Lammers, A. M. Sofias, *J. Controlled Release* **2020**, *328*, 805.
- [30] D. J. Vugts, C. Klaver, C. Sewing, A. J. Poot, K. Adamzek, S. Huegli, C. Mari, G. W. M. Visser, I. E. Valverde, G. Gasser, T. L. Mindt, G. van Dongen, *Eur. J. Nucl. Med. Mol. Imaging* **2017**, *44*, 286.
- [31] R. Boellaard, *J. Nucl. Med.* **2018**, *59*, 1753.
- [32] N. E. Makris, R. Boellaard, E. P. Visser, J. R. de Jong, B. Vanderlinden, R. Wierds, B. J. van der Veen, H. J. Greuter, D. J. Vugts, G. A. van Dongen, A. A. Lammertsma, M. C. Huisman, *J. Nucl. Med.* **2014**, *55*, 264.
- [33] Y. W. S. Jauw, F. Bensch, A. H. Brouwers, O. S. Hoekstra, J. M. Zijlstra, S. Pieplenbosch, C. P. Schroder, S. Zweegman, G. van Dongen, C. W. Menke-van der Houven van Oordt, E. G. E. de Vries, H. C. W. de Vet, R. Boellaard, M. C. Huisman, *Eur. J. Nucl. Med. Mol. Imaging* **2019**.